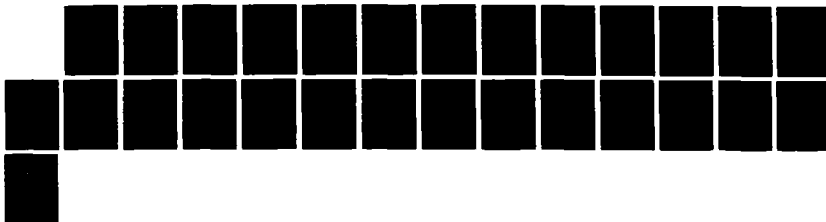
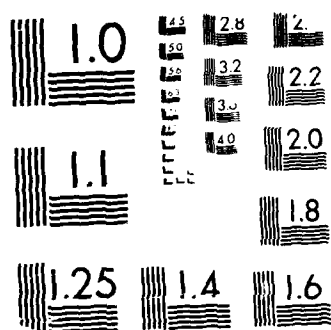


AD-A193 005 NASCENT VIBRATIONAL/ROTATIONAL DISTRIBUTION PRODUCED BY 1/1  
HYDROGEN ATOM REC. (U) AEROSPACE CORP EL SEGUNDO CA  
AEROPHYSICS LAB A O WOODIN 01 FEB 60  
UNCLASSIFIED TR-0006A(2930-02)-1 SD-TR-07-61 F/G 20/5 NL





MICROCOPY RESOLUTION TEST CHART  
 NATIONAL BUREAU OF STANDARDS-1963-A

AD-A193 005

Nascent Vibrational/Rotational Distribution  
Produced by Hydrogen Atom Recombination

A. O. WOODIN  
Aerophysics Laboratory  
Laboratory Operations  
The Aerospace Corporation  
El Segundo, CA 90245

1 February 1988

Prepared for  
SPACE DIVISION  
AIR FORCE SYSTEMS COMMAND  
Los Angeles Air Force Base  
P.O. Box 92960, Worldway Postal Center  
Los Angeles, CA 90009-2960

APPROVED FOR PUBLIC RELEASE;  
DISTRIBUTION UNLIMITED

DTIC  
ELECTE  
MAR 18 1988  
S H D

88 3 16 094

This report was submitted by the Aerospace Corporation, El Segundo, CA 90245, under Contract No. F04701-85-C-0086-P00016 with the Space Division, P.O. Box 92960, Worldway Postal Center, Los Angeles, CA 90009-2960. It was reviewed and approved for The Aerospace Corporation by W. P. Thompson, Director, Aerophysics Laboratory.

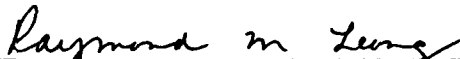
Lt John Abreu/WCO was the project officer for the Mission-Oriented Investigation and Experimentation (MOIE) Program.

This report has been reviewed by the Public Affairs Office (PAS) and is releasable to the National Technical Information Service (NTIS). At NTIS, it will be available to the general public, including foreign nationals.

This technical report has been reviewed and is approved for publication. Publication of this report does not constitute Air Force approval of the report's findings or conclusions. It is published only for the exchange and stimulation of ideas.



JOHN ABREU, Lt, USAF  
MOIE Project Officer  
AFSTC/WCO OL-AB



RAYMOND M. LEONG, Major, USAF  
Deputy Director, AFSTC West Coast  
Office  
AFSTC/WCO OL-AB

UNCLASSIFIED

SECURITY CLASSIFICATION OF THIS PAGE

A193 005

## REPORT DOCUMENTATION PAGE

1a. REPORT SECURITY CLASSIFICATION Unclassified			1b. RESTRICTIVE MARKINGS		
2a. SECURITY CLASSIFICATION AUTHORITY			3. DISTRIBUTION/AVAILABILITY OF REPORT Approved for public release; distribution unlimited		
2b. DECLASSIFICATION/DOWNGRADING SCHEDULE			5. MONITORING ORGANIZATION REPORT NUMBER(S) SD-TR-87-61		
4. PERFORMING ORGANIZATION REPORT NUMBER(S) TR-0086A(2930-02)-1			7a. NAME OF MONITORING ORGANIZATION Space Division		
6a. NAME OF PERFORMING ORGANIZATION The Aerospace Corporation Laboratory Operations		6b. OFFICE SYMBOL (If applicable)	7b. ADDRESS (City, State, and ZIP Code) Los Angeles Air Force Base Los Angeles, CA 90009-2960		
6c. ADDRESS (City, State, and ZIP Code) El Segundo, CA 90245		9. PROCUREMENT INSTRUMENT IDENTIFICATION NUMBER F04701-85-C-0086-P00016			
8a. NAME OF FUNDING/SPONSORING ORGANIZATION		8b. OFFICE SYMBOL (If applicable)	10. SOURCE OF FUNDING NUMBERS		
8c. ADDRESS (City, State, and ZIP Code)		PROGRAM ELEMENT NO. PROJECT NO. TASK NO. WORK UNIT ACCESSION NO.			
11. TITLE (Include Security Classification) Nascent Vibrational/Rotational Distribution Produced by Hydrogen Atom Recombination					
12. PERSONAL AUTHOR(S) Woodin, Ann O.					
13a. TYPE OF REPORT		13b. TIME COVERED FROM TO		14. DATE OF REPORT (Year, Month, Day) 1 February 1988	
15. PAGE COUNT 23		16. SUPPLEMENTARY NOTATION			
17. COSATI CODES			18. SUBJECT TERMS (Continue on reverse if necessary and identify by block number)		
FIELD	GROUP	SUB-GROUP	Frozen-Flow Losses, Hydrogen, Nascent Distribution Quasiclassical Calculation, Recombination, State-to- State Rate Coefficients, Vibrational/Rotational Distribution		
19. ABSTRACT (Continue on reverse if necessary and identify by block number)					
The nascent vibrational/rotational distribution produced by the reaction $H + H + H + H_2(v, J) + H$ is calculated using resonance complex theory. The calculations are performed using the accurate Siegbahn-Liu-Truhlar-Horowitz surface. Results are presented for the dependence of the total recombination rate coefficient on temperature, and specific rate coefficients into individual vibrational/rotational states.					
20. DISTRIBUTION/AVAILABILITY OF ABSTRACT <input type="checkbox"/> UNCLASSIFIED/UNLIMITED <input checked="" type="checkbox"/> SAME AS RPT. <input type="checkbox"/> DTIC USERS			21. ABSTRACT SECURITY CLASSIFICATION Unclassified		
22a. NAME OF RESPONSIBLE INDIVIDUAL			22b. TELEPHONE (Include Area Code)		22c. OFFICE SYMBOL

# PREFACE

This program was initiated with support from J. Pollard and R. Cohen. L. Friesen and C. Randall contributed computer time on the DIRAC Vax facility. Most of the calculations were performed on the Aerophysics Laboratory Microvax System (ALMS).



Accession For	
NTIS GRA&I	<input checked="" type="checkbox"/>
DTIC TAB	<input type="checkbox"/>
Unannounced	<input type="checkbox"/>
Justification	
By	
Distribution/	
Availability Codes	
Dist	Avail and/or Special
A-1	

## CONTENTS

PREFACE.....	1
I. INTRODUCTION.....	7
II. COMPUTATIONAL DETAILS.....	9
III. RESULTS.....	15
IV. CONCLUSIONS.....	25
REFERENCES.....	27

## FIGURES

1.	Probabilities for Final Vibrational/Rotational State Formed from Initial Resonance State $v = 13$ , $J = 8$ for Initial $E/k = 50$ K.....	16
2.	Probabilities for Vibrational/Rotational State Formed from Initial Resonance State $v = 13$ , $J = 8$ for Initial $E/k = 1000$ K.....	17
3.	Vibrational Cross Sections Formed from Initial Resonance State $v = 13$ , $J = 8$ .....	18
4.	Total Recombination Rate Constant as a Function of Temperature.....	19
5.	Rate Constants into Given Final Vibrational State as a Function of Temperature.....	20
6.	Rate Constants into Given Final Rotational State for Final $v = 14$ as a Function of Temperature.....	21
7.	Rate Constants into Given Final Rotational State for Final $v = 13$ as a Function of Temperature.....	23

## TABLE

1.	Properties of Six Resonance States in Recombination Calculation.....	11
----	--	----



## I. INTRODUCTION

For almost 50 years there has been great experimental<sup>1-8</sup> and theoretical<sup>9-18</sup> interest in the gas-phase recombination of hydrogen, the process



Reaction (1), where  $\text{M} = \text{H}$ , represents one of the simplest chemical reactions and is of fundamental interest to chemical dynamics and astrophysics. Indeed, this reaction tests the outer limits of the  $(\text{H})_3$  potential energy surface. This reaction is of particular interest because of the recent calculations and experiments on the similar  $\text{H} + \text{D}_2$  system.<sup>19-22</sup> The comparison of theory and experiment in these simple three-electron systems tests our ability to understand chemical reactions.

Recombination of hydrogen is of practical importance in both plasma physics and rocket propulsion, especially for hybrid and electrothermal propulsion systems.<sup>23,24</sup> This reaction becomes important in chemical rockets if hydrogen is a major atomic component of the fuel. In these systems, the total recombination rate coefficient and the distribution of energy into the product vibrational/rotational states are important. For efficient propulsion, the translational energy of the exhaust must be maximized. Frozen flow efficiency losses occur when the molecules do not sustain enough collisions in the nozzle to equilibrate the translational and vibrational/rotational degrees of freedom. The energy that is trapped in the vibrational/rotational modes of the system is not available for thrust.

Experimental reaction rate data were critically reviewed by Baulch et al. in 1972<sup>25</sup> and by Cohen and Westberg in 1982.<sup>26</sup> For many third bodies, including  $\text{M} = \text{H}_2$ , He, and Ar, accurate measurements<sup>4,5</sup> and accurate calculations<sup>17</sup> are available and are in reasonable agreement. For  $\text{M} = \text{H}$ , there is a lack of reliable experimental data. Shock tube measurements at high temperatures have been performed but have not been very reproducible.<sup>25,26</sup> At lower temperatures, only an upper limit to the rate coefficient at 300 K is available, which was obtained by Bennett and Blackmore.<sup>2</sup> This upper limit is not in

agreement with the theoretical result,<sup>12,17</sup> and the experimental method has been questioned by Baulch et al.<sup>25</sup>

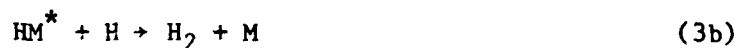
The nascent vibrational/rotational product state distribution of recombined  $H_2$  has never been measured. In this report, we present a calculation of this distribution using resonance complex theory. The theory and computational details are described in Section II. The total recombination rate coefficient is presented and compared to previous calculations in Section III. The nascent vibrational/rotational distribution is discussed, and rate coefficients into individual vibrational/rotational states as functions of temperature are presented.

## II. COMPUTATIONAL DETAILS

A three-body recombination process can take place primarily via two separate channels: the "energy-transfer" mechanism



and the "exchange" or "chaperone" mechanism



where  $\text{H}_2^*$  and  $\text{HM}^*$  are intermediate (unbound) complexes that are in equilibrium. In the present case, where  $\text{M} = \text{H}$ , the two processes can be distinguished in a classical calculation; quantum mechanically these two channels are indistinguishable.

The resonance complex theory of Roberts, Bernstein, and Curtiss<sup>11</sup> is used to study the recombination process. Because this theory has been discussed in detail elsewhere, only a brief description follows. In this theory, the complex  $[\text{H}_2^*]$  in Eq. (2)] is identified with orbiting resonance states of the  $\text{H}_2$  system. These states are bound classically but have a finite lifetime quantum mechanically, because of tunneling. We assume that some of these states reach a steady-state population distribution determined by their equilibrium constant. Hence the reaction rate can be written as a sum over individual rate constants

$$k_r(v, J, T) = \sum_i k_r^i(v, J, T) \quad (4)$$

The individual rate coefficient for deactivation of an orbiting resonance  $i$  can be expressed as

$$k_r^i(v, J, T) = \bar{v}_r K_{eq}^i \bar{\sigma}_i^-(v, J, T) \quad (5)$$

where

$$\bar{v}_r = (8kT/\pi\mu)^{1/2} \quad (6)$$

$K_{eq}^i$  is the equilibrium constant for the formation of the  $i^{th}$  resonance complex state,  $\mu$  is the reduced mass for the ( $H_2M$ ) system, and

$$\bar{\sigma}_i(v, J, T) = (kT)^{-2} \int_0^{\infty} E \sigma_i(v, J, E) \exp(-E/kT) dE \quad (7)$$

is the thermal average of the energy dependent, state-selective, cross section.

To calculate vibrational/rotational rate coefficients, the resonance states contributing to the hydrogen ( $H + H + H$ ) recombination process must be determined. There are approximately 50 orbiting resonance states of  $H_2$ .<sup>27,28</sup> The procedure for assessing the contribution of each resonance state was discussed in the first calculation using resonance complex theory.<sup>11</sup> Most of these states can be eliminated by simple energy considerations because the equilibrium constant contains a factor of  $\exp(-E/kT)$ . The majority of the remaining states (about 15) have lifetimes much too long (i.e., too narrow in resonance width) to contribute to the recombination. The result is 6 possible contributing orbiting resonance states. The properties of these states are summarized in Table 1. The literature includes discussions about which of these 6 resonance states contributes to recombination under various experimental conditions.<sup>6,8</sup> We decided to calculate contributions from all 6 states. If it is determined that, under certain experimental conditions, some of the states do not contribute or are not in complete thermal equilibrium, they could then easily be excluded from the final calculation of the rate coefficient.

Table 1. Properties of Six Resonance States in Recombination Calculation

$v$	$J$	$E_i (\text{cm}^{-1})$	$\langle R \rangle (\text{au})$	$\tau_i (\text{sec})$
14	5	45.7	6.51	$2.7 \times 10^{-13}$
14	4	3.6	6.05	$4.0 \times 10^{-10}$
13	8	89.8	5.31	$2.0 \times 10^{-12}$
12	11	216.0	4.86	$1.8 \times 10^{-12}$
12	12	387.0	5.30	$7.0 \times 10^{-14}$
11	13	199.5	4.27	$2.0 \times 10^{-9}$

Two of the resonance states require an additional approximation. The  $v = 14$ ,  $J = 5$  and the  $v = 12$ ,  $J = 12$  states are classically unbound. In order to carry out classical trajectories with these initial states, it is therefore necessary to select them to be slightly classically bound, that is, with a slightly lower internal energy. The vibrational quantum number defined by<sup>29</sup>

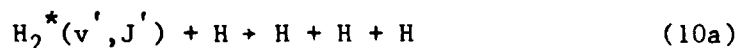
$$v = -1/2 + (1/\pi\hbar) \int_{R_-}^{R_+} \{2m[E_{\text{int}} - V(R) - (J_r J_r / 2mR^2)]\}^{1/2} dR \quad (8)$$

where  $R_{\pm}$  are the diatomic turning points,  $E_{\text{int}}$  is the internal energy,  $V(R)$  is the diatomic potential energy,  $m$  is the diatomic reduced mass, and  $J_r$  is related to the rotational quantum number by

$$J_r^2 = j(j+1)\hbar^2 \quad (9)$$

then takes on noninteger values. The "vibrational quantum number" for the  $v = 14$  resonance state is  $v = 13.85$  and for the  $v = 12$  state is  $v = 11.72$ . To assess the effects of this change, calculations are run for not only these two states but also for other nearby ( $E_{\text{int}}$  slightly different) states. No effect is found either on the total cross section or on the final vibrational/rotational state distribution.

Once the resonance state is selected, quasiclassical trajectories are calculated for the process



to converge  $\sigma_1(v, J, E)$ . A similar calculation with  $M = \text{H}, \text{He}, \text{Ar}$ , and  $\text{H}_2$  was performed by Whitlock et al.<sup>17</sup> for the total recombination rate coefficient. The present calculation follows the same basic procedure. However, several changes were needed to determine the vibrational/rotational distribution of products. Classical trajectories on the  $(\text{H})_3$  potential energy surface used by Whitlock et al.<sup>17</sup> were calculated using CLASTR.<sup>30</sup> We discovered that the surface supports many bound vibrational/rotational states that are unbound for the true  $\text{H}_2$  system. A highly accurate surface for  $\text{H}_3$  is available, the

SLTH<sup>31,32</sup> surface. Therefore, we modified CLASTR to accept this surface and to determine the final vibrational and rotational state quantum number for the SLTH surface. We constructed the correct initial conditions for the trajectories based on the orbiting resonance state and calculated the final vibrational and rotational quantum numbers. The procedure is similar to the one described by Truhlar and Muckerman<sup>29</sup> and will not be reviewed. Because of the highly excited states encountered for both the initial and final conditions, we made one modification to their described procedure. The Newton-Raphson iteration technique, to locate the turning points of the effective potential, was replaced with the method of Pade approximates.

After the individual vibrational/rotational cross section has been calculated as a function of E, it is then fitted to the form

$$\sigma_i(E, v, J) = b(E/k)^{-1/2} \exp[-a(E/k)^{-1}] \quad (11)$$

as suggested by Whitlock et al. After thermal averaging to determine  $\bar{\sigma}_i(v, J, T)$ , the cross sections are combined to produce the rate coefficient for the desired vibrational/rotational state.

For each of the six resonance states, five energies are calculated ( $E/k = 50, 100, 300, 1000, \text{ and } 2000 \text{ K}$ ). This is found to be adequate to calculate the thermally averaged cross section. For each energy and initial resonance state, approximately 1000 trajectories were run, producing a Monte Carlo error of less than 5% for the total cross section, of approximately 10% for the summed vibrational cross sections, and of approximately 20% for the individual vibrational/rotational cross sections.

### III. RESULTS

The individual final state vibrational/rotational probabilities for one initial resonance state,  $v = 13$ ,  $J = 8$ , are shown for  $E/k = 50$  K in Fig. 1 and for  $E/k = 1000$  K in Fig. 2. The qualitative features are the same for all the resonance states. The dissociation level for the hydrogen molecule is shown by the heavy line in the figures. The figures indicate that the distribution is peaked near this line, that is, in the highest bound states of the  $H_2$  manifold. The distribution broadens and extends to lower vibrational states as the collision energy increases. The total reaction probability decreases with increasing energy. Figure 3 exhibits the individual vibrational cross sections for the same intermediate state as functions of collision energy. Again, the qualitative features are the same for all resonance states. In this figure, the widening of the vibrational distribution and the falloff of the total cross section with increasing collision energy can be seen clearly. (Space considerations preclude the display of all the individual vibrational/rotational cross sections as functions of energy. The complete results are available on request.) The nascent vibrational/rotational distribution is the correctly weighted sum over the individual orbiting resonance states.

In Fig. 4, the results for the total rate coefficient as a function of temperature are plotted and compared with the calculation of Whitlock et al.<sup>17</sup> The two data sets reveal the same qualitative behavior with temperature. However, the present results are approximately a factor of 2 smaller than the previous results. This difference occurs because the potential energy surface used by Whitlock et al.<sup>17</sup> binds too many vibrational/rotational states, as discussed previously. In Fig. 5, the rate coefficients into individual vibrational states are plotted and compared with the total rate coefficient and with the sum over the plotted states. This figure indicates that  $v = 14$ ,  $v = 13$ ,  $v = 12$ , and  $v = 11$  make up the largest contribution to the rate coefficient. Figure 5 also exhibits the broadening of the distribution with energy, with  $v = 14$  dominating the rate constant at lower temperatures but becoming overshadowed by  $v = 13$  at higher temperatures. Figure 6 displays the rotational rate coefficients for  $v = 14$ . The higher rotational levels



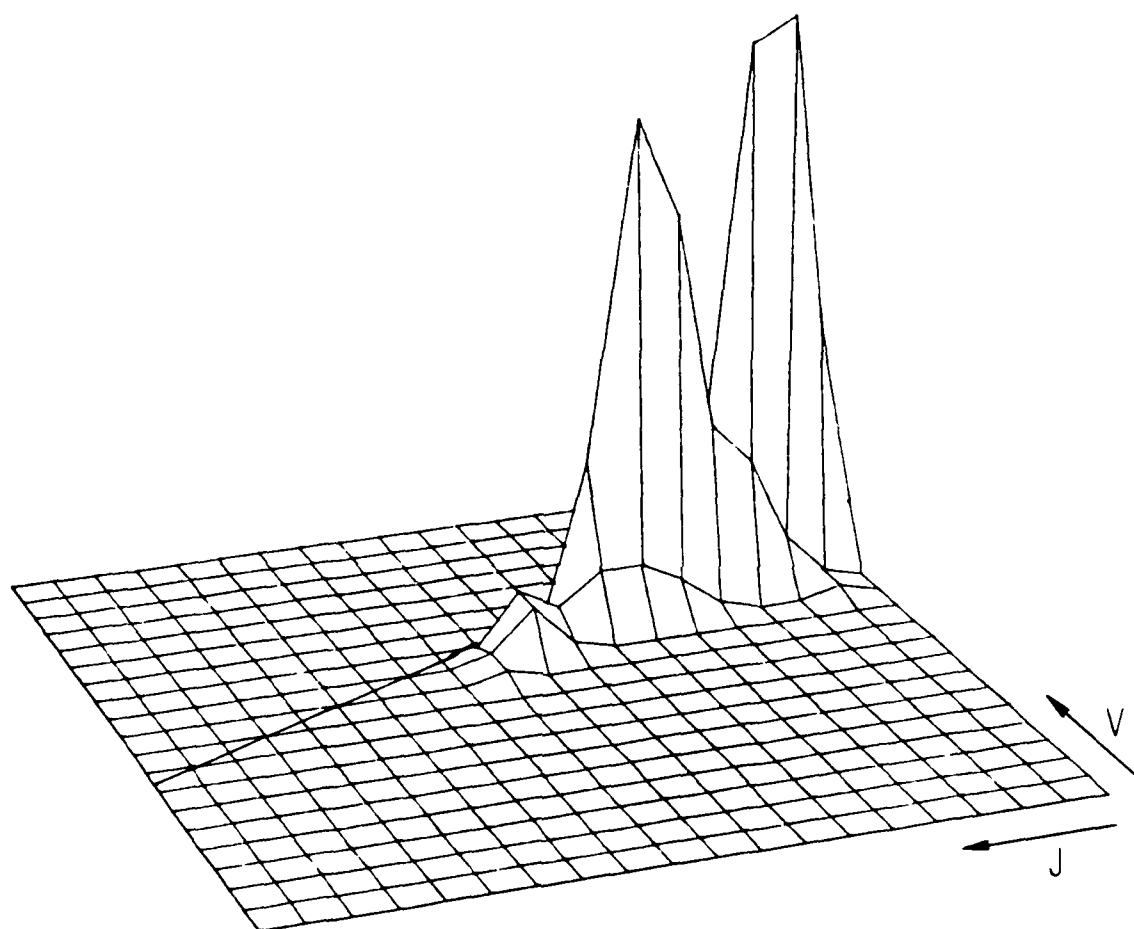


Fig. 1. Probabilities for Final Vibrational/Rotational State Formed from Initial Resonance State  $v = 13, J = 8$  for Initial  $E/k = 50$  K

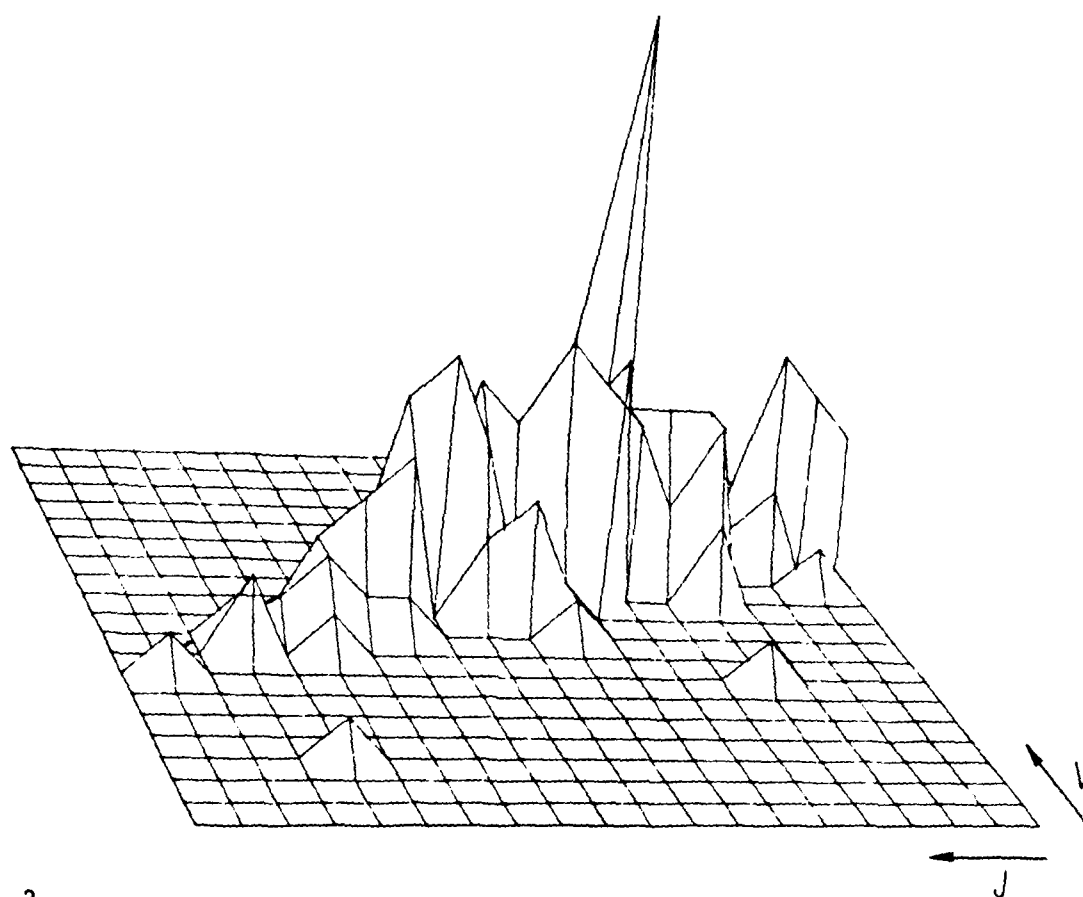


Fig. 2. Probabilities for Final Vibrational/Rotational State Formed from Initial Resonance State  $v = 13$ ,  $J = 8$  for Initial  $E/k = 1000$  K

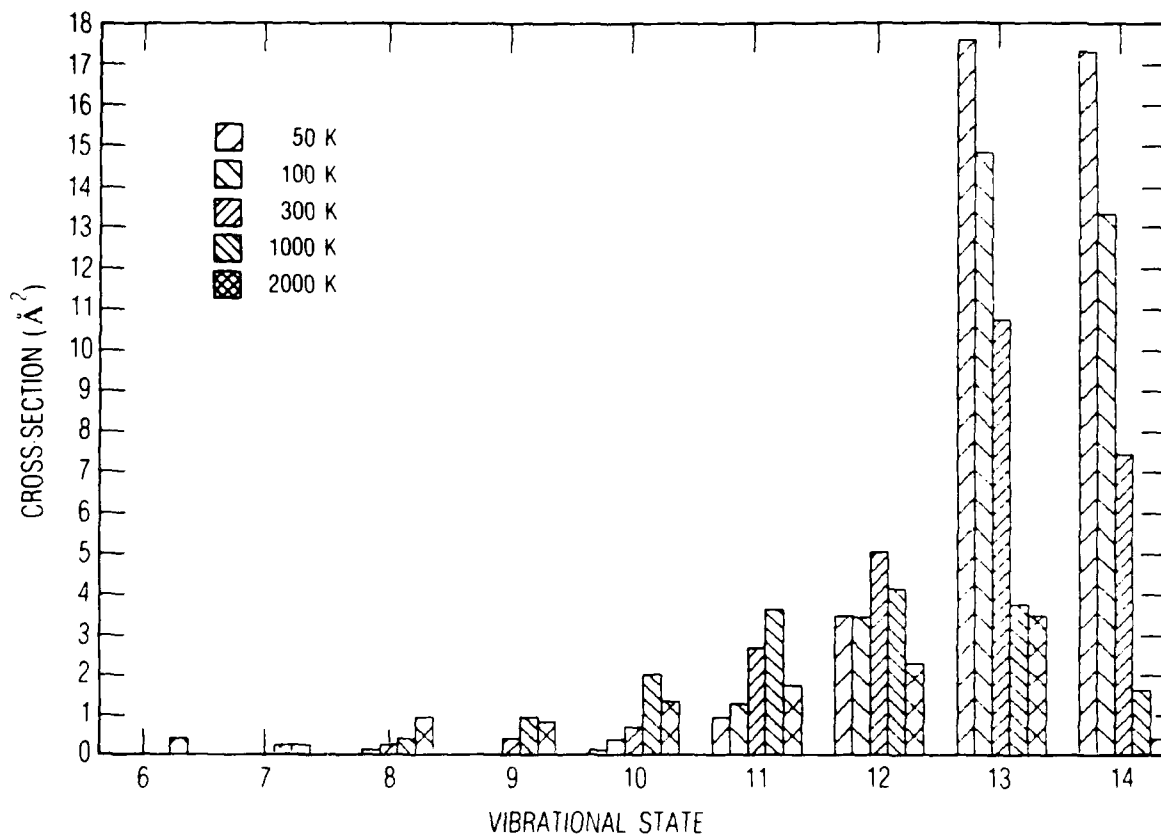


Fig. 3. Vibrational Cross Sections Formed from Initial Resonance State  $v = 13$ ,  $J = 8$

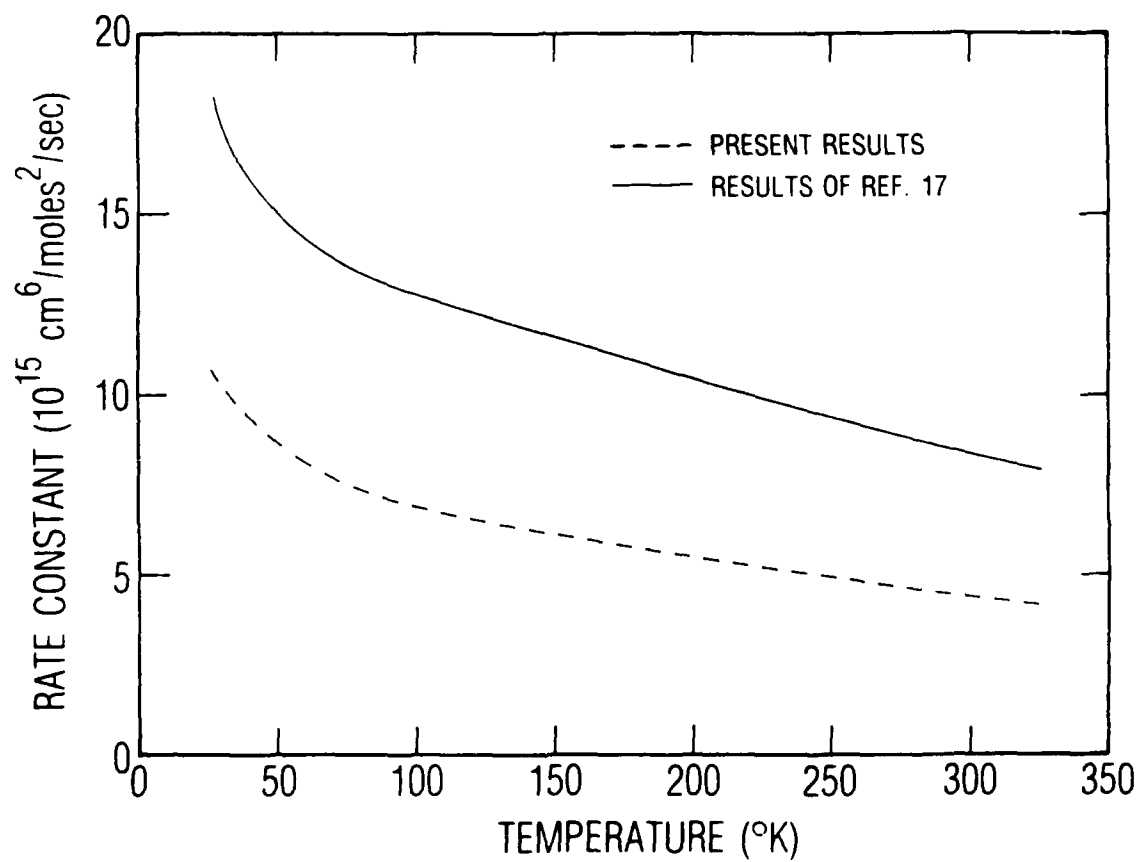


Fig. 4. Total Recombination Rate Constant as a Function of Temperature

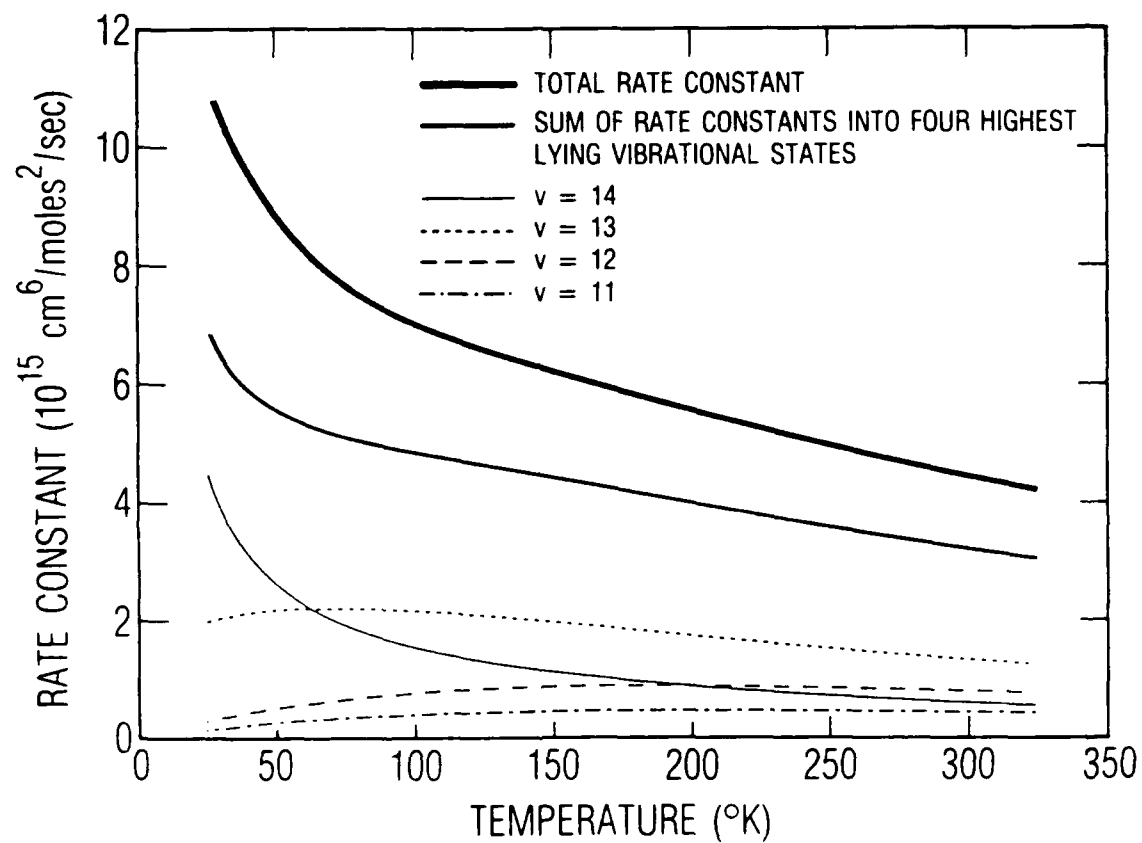


Fig. 5. Rate Constants into Given Final Vibrational State as a Function of Temperature

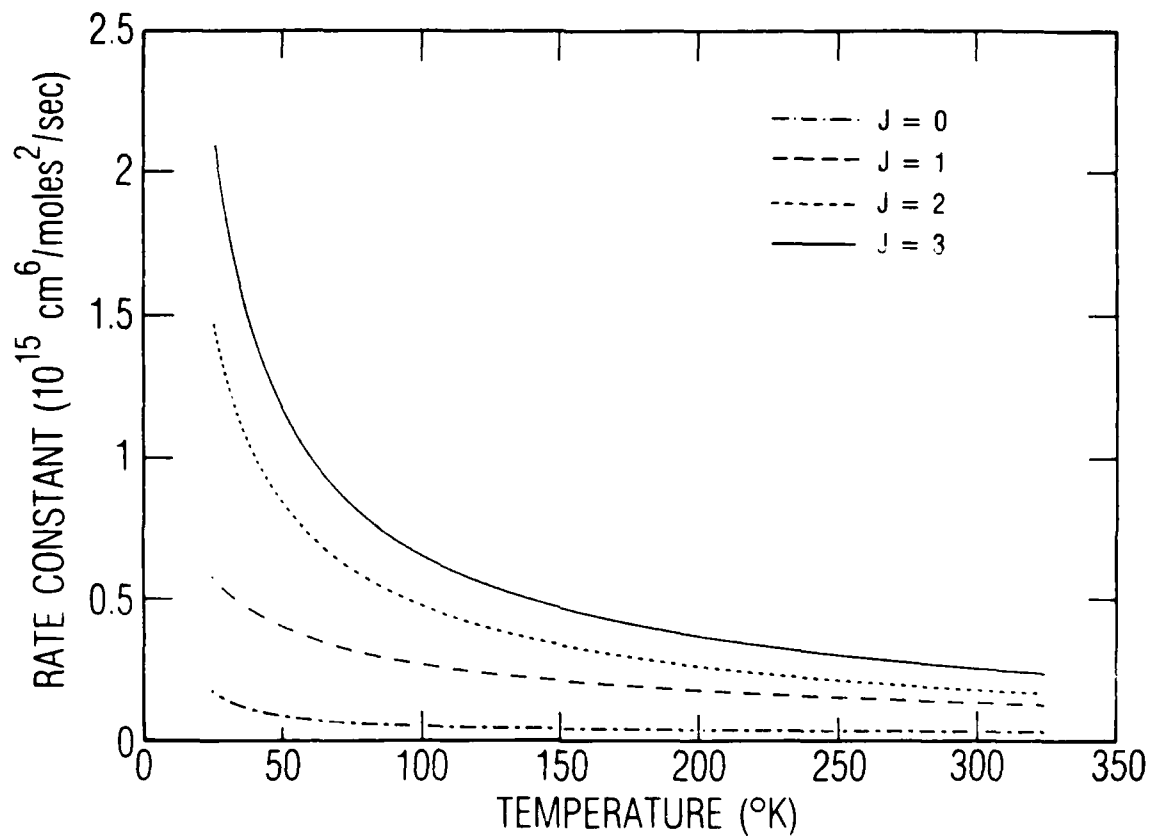


Fig. 6. Rate Constants into Given Final Rotational State for Final  $v = 14$  as a Function of Temperature

dominate;  $J = 3$  is the highest bound state for  $v = 14$ . Figure 7 exhibits the rotational rate coefficients for  $v = 13$ . Again, the higher rotational states dominate, with the highest four states constituting approximately 80% of the total rate coefficients. ( $J = 7$  is the highest bound state for  $v = 13$ .)

These results indicate that the nascent vibrational/rotational distribution peaks in the highest bound states of the hydrogen molecule. The average vibrational level is high. Because such high vibrational states can only support a small number of bound rotational states, the average rotational level is small.

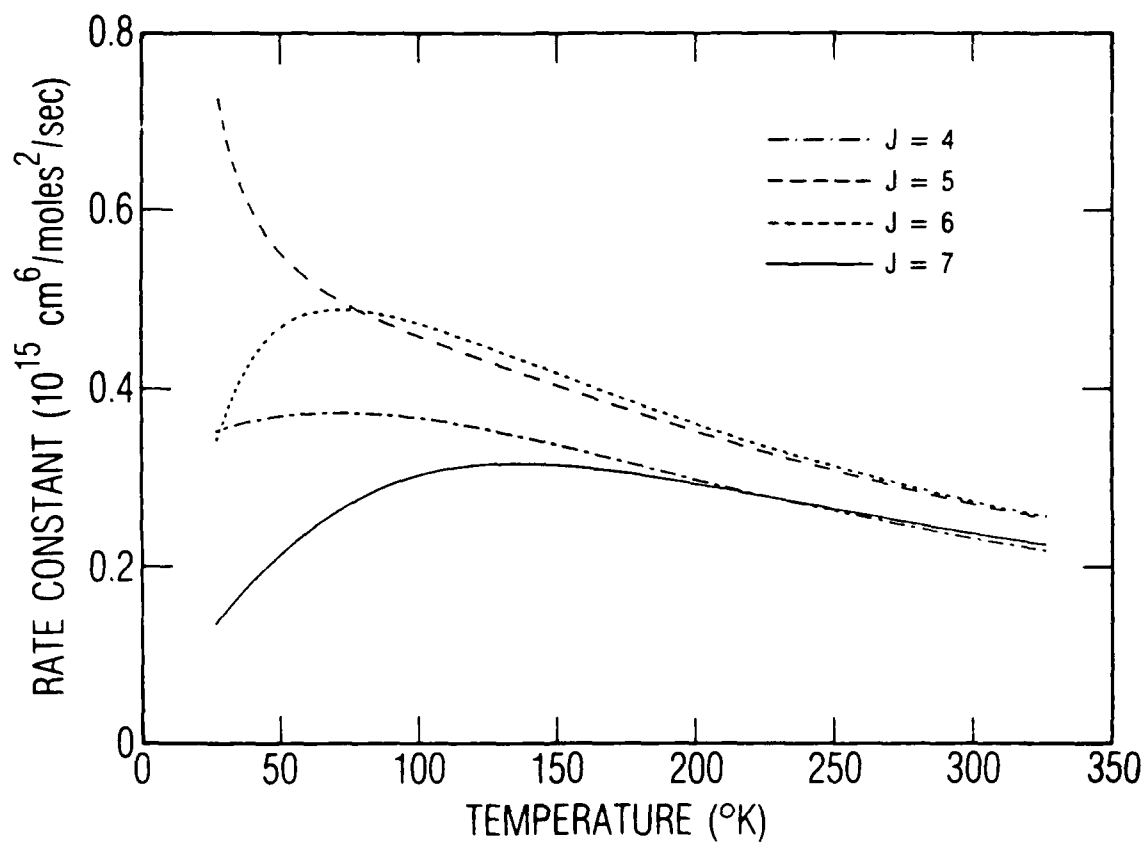


Fig. 7. Rate Constants into Given Final Rotational State for Final  $v = 13$  as a Function of Temperature



#### IV. CONCLUSIONS

We have used resonance complex theory to investigate the nascent vibrational/rotational state distribution produced by hydrogen atom recombination. We have shown that this distribution peaks in the highest bound states of the hydrogen molecule. Because of the highly excited nature of the products, the nascent distribution is greatly changed by subsequent collisions. To assess the effect of a collision on the distribution, calculations must be performed to determine the rate constant for dissociation and relaxation from these states. This is particularly important when inert third bodies such as helium are considered. The measured hydrogen ortho/para ratio in such systems may not be the nascent distribution because of the effect of vibrationally enhanced exchange reactions.

This state distribution was calculated using the approximations of quasi-classical theory. Though a correct quantum-mechanical state was used for initial conditions, the subsequent collision was treated using classical mechanics. As has been previously discussed, classical results are more accurate the greater the degree of averaging in the calculation.<sup>29</sup> Therefore we would expect the total rate coefficient to have the greatest accuracy, the vibrational rate constants to be less accurate, and the individual vibrational/rotational rate constants to be the least accurate. The qualitative features of the distribution should be correct, that is, the distribution is almost certainly peaked in the highest states of the bound hydrogen molecule.

Future calculations will address the effects of a collision on the nascent distributions and will investigate the nascent vibrational/rotational distribution produced with an inert third body such as helium. We hope that the results will be more readily subject to experimental test.

# REFERENCES

1. I. Amdur, J. Am. Chem. Soc. **60**, 2347 (1938).
2. J. E. Bennett and D. R. Blackmore, Proc. R. Soc. A **305**, 553 (1968).
3. F. S. Larkin, Can. J. Chem. **46**, 1005 (1968).
4. D. O. Ham, D. W. Trainor, and F. Kaufman, J. Chem. Phys., **53**, 4395 (1970).
5. L. P. Walkauskas and F. Kaufman, Fifteenth Symposium (International) on Combustion, The Combustion Institute, Pittsburgh (1975), p. 691.
6. L. P. Walkauskas and F. Kaufman, J. Chem. Phys. **64**, 3885 (1976).
7. K. P. Lynch, T. C. Schwab, and J. V. Michael, Int. J. of Chem. Kin. **8**, 651 (1976).
8. D. N. Mitchell and D. J. LeRoy, J. Chem. Phys. **67**, 1042 (1977).
9. J. C. Keck, J. Chem. Phys. **32**, 1035 (1960).
10. D. L. Bunker, J. Chem. Phys. **32**, 1001 (1960).
11. R. E. Roberts, R. B. Bernstein, and C. F. Curtiss, J. Chem. Phys. **50**, 5163 (1969).
12. V. H. Shui and J. P. Appleton, J. Chem. Phys. **55**, 3126 (1971).
13. R. T. Pack, R. L. Snow, and W. D. Smith, J. Chem. Phys. **56**, 926 (1972).
14. P. A. Whitlock, J. T. Muckerman, and R. E. Roberts, Chem. Phys. Lett. **16**, 460 (1972).
15. A. Jones and J. L. J. Rosenfeld, Proc. R. Soc. A **333**, 419 (1973).
16. V. H. Shui, J. Chem. Phys. **58**, 4868 (1973).
17. P. A. Whitlock, J. T. Muckerman, and R. E. Roberts, J. Chem. Phys. **60**, 3658 (1974).
18. J. Troe, Ann. Rev. Phys. Chem. **29**, 223 (1978).
19. E. E. Marinero, C. T. Rettner, and R. N. Zare, J. Chem. Phys. **80**, 4142 (1984).
20. D. P. Gerrity and J. J. Valentini, J. Chem. Phys. **79**, 5205 (1983); **81**, 1296 (1984); **82**, 1323 (1985).

21. R. Goetting, H. R. Mayne, and J. P. Toennies, J. Chem. Phys. **80**, 2230 (1984).
22. N. C. Blais and D. G. Truhlar, Chem. Phys. Lett. **102**, 120 (1983).
23. J. E. Pollard and R. B. Cohen, J. of Prop. and Power **2**, 124 (1986).
24. K. Flurchick and R. D. Etters, AIAA J. **23**, 981 (1985).
25. D. L. Baulch, D. D. Drysdale, D. G. Horne, and A. C. Lloyd, Evaluated Kinetic Data For High Temperature Reactions, Vol. I, Butterworths, London (1972).
26. N. Cohen and K. R. Westberg, Chemical Kinetic Data Sheets for High-Temperature Chemical Reactions, ATR-82(7888)-3, The Aerospace Corporation, El Segundo, Calif. (15 July 1982).
27. T. G. Waech and R. B. Bernstein, J. Chem. Phys. **46**, 4905 (1967).
28. R. J. LeRoy and R. B. Bernstein, J. Chem. Phys. **55**, 5114 (1971).
29. D. G. Truhlar and J. T. Muckerman, Atom-Molecule Collision Theory, ed. R. B. Bernstein, Plenum Press, New York (1979) p. 505.
30. J.T. Muckerman, QCPE **11**, 229 (1973).
31. P. Siegbahn and B. Liu, J. Chem. Phys. **68**, 2457 (1978).
32. D. G. Truhlar and C. J. Horowitz, J. Chem. Phys. **68**, 2466 (1978).

## LABOPATORY OPERATIONS

The Aerospace Corporation functions as an "architect-engineer" for national security projects, specializing in advanced military space systems. Providing research support, the corporation's Laboratory Operations conducts experimental and theoretical investigations that focus on the application of scientific and technical advances to such systems. Vital to the success of these investigations is the technical staff's wide-ranging expertise and its ability to stay current with new developments. This expertise is enhanced by a research program aimed at dealing with the many problems associated with rapidly evolving space systems. Contributing their capabilities to the research effort are these individual laboratories:

Aerophysics Laboratory: Launch vehicle and reentry fluid mechanics, heat transfer and flight dynamics; chemical and electric propulsion, propellant chemistry, chemical dynamics, environmental chemistry, trace detection; spacecraft structural mechanics, contamination, thermal and structural control; high temperature thermomechanics, gas kinetics and radiation; cw and pulsed chemical and excimer laser development including chemical kinetics, spectroscopy, optical resonators, beam control, atmospheric propagation, laser effects and countermeasures.

Chemistry and Physics Laboratory: Atmospheric chemical reactions, atmospheric optics, light scattering, state-specific chemical reactions and radiative signatures of missile plumes, sensor out-of-field-of-view rejection, applied laser spectroscopy, laser chemistry, laser optoelectronics, solar cell physics, battery electrochemistry, space vacuum and radiation effects on materials, lubrication and surface phenomena, thermionic emission, photo-sensitive materials and detectors, atomic frequency standards, and environmental chemistry.

Computer Science Laboratory: Program verification, program translation, performance-sensitive system design, distributed architectures for spaceborne computers, fault-tolerant computer systems, artificial intelligence, micro-electronics applications, communication protocols, and computer security.

Electronics Research Laboratory: Microelectronics, solid-state device physics, compound semiconductors, radiation hardening; electro-optics, quantum electronics, solid-state lasers, optical propagation and communications; microwave semiconductor devices, microwave/millimeter wave measurements, diagnostics and radiometry, microwave/millimeter wave thermionic devices; atomic time and frequency standards; antennas, rf systems, electromagnetic propagation phenomena, space communication systems.

Materials Sciences Laboratory: Development of new materials: metals, alloys, ceramics, polymers and their composites, and new forms of carbon; non-destructive evaluation, component failure analysis and reliability; fracture mechanics and stress corrosion; analysis and evaluation of materials at cryogenic and elevated temperatures as well as in space and enemy-induced environments.

Space Sciences Laboratory: Magnetospheric, auroral and cosmic ray physics, wave-particle interactions, magnetospheric plasma waves; atmospheric and ionospheric physics, density and composition of the upper atmosphere, remote sensing using atmospheric radiation; solar physics, infrared astronomy, infrared signature analysis; effects of solar activity, magnetic storms and nuclear explosions on the earth's atmosphere, ionosphere and magnetosphere; effects of electromagnetic and particulate radiations on space systems; space instrumentation.

END

DATE

FILMED

DTIC

JULY 88